Two-Dimensional particle-in-cell simulations of the nonresonant, cosmic-ray driven instability in SNR shocks

Yutaka Ohira[1], Brian Reville[2], John G. Kirk[2] and Fumio Takahara[1]

ABSTRACT

In supernova remnants, the nonlinear amplification of magnetic fields upstream of collisionless shocks is essential for the acceleration of cosmic rays to the energy of the "knee" at $10^{15.5}$ eV. A nonresonant instability driven by the cosmic ray current is thought to be responsible for this effect. We perform two-dimensional, particle-in-cell simulations of this instability. We observe an initial growth of circularly polarized non-propagating magnetic waves as predicted in linear theory. It is demonstrated that in some cases the magnetic energy density in the growing waves, can grow to at least 10 times its initial value. We find no evidence of competing modes, nor of significant modification by thermal effects. At late times we observe saturation of the instability in the simulation, but the mechanism responsible is an artefact of the periodic boundary conditions and has no counterpart in the supernova-shock scenario.

Subject headings: supernova remnants – shock waves – plasmas – cosmic rays

1. Introduction

Diffusive shock acceleration (DSA) at supernova remnant shocks is widely considered to be the primary source of galactic cosmic rays (for a recent review see Hillas 2005). A crucial aspect of DSA is the self-excitation of hydromagnetic waves due to currents produced by the streaming energetic ions. These provide the pitch-angle scattering necessary to allow spatial diffusion of the relativistic particles. The maximum acceleration rate that can be obtained corresponds to the smallest possible spatial diffusion coefficient. In this 'Bohm limit' the maximum particle energy is determined either by the age of the remnant (Lagage & Cesarsky 1983), or by its geometry (Berezhko 1996). Even adopting optimistic values for the upstream

[1]Department of Earth and Space Science, Graduate School of Science, Osaka University, 1-1 Machikaneyama-cho, Toyonaka, Osaka 560-0043, Japan; yutaka@vega.ess.sci.osaka-u.ac.jp

[2]Max-Planck-Institut für Kernphysik, Heidelberg 69029, Germany

parameters of a supernova remnant shock, particles are limited to energies below the knee of the cosmic-ray spectrum at $\sim 10^{15.5}$ eV. However, nonlinear amplification of the upstream magnetic field due to cosmic-ray currents may provide a possible solution to this problem (Shapiro et al. 1998; Lucek & Bell 2000).

There is increasing observational evidence that the magnetic fields immediately downstream of several young supernova remnant shocks are much stronger than would be obtained by compressing the ambient interstellar field at an MHD shock front (Vink & Laming 2003; Berezhko et al. 2003; Bamba et al. 2005; Uchiyama et al. 2007). These observations give additional motivation to the development of theoretical models of nonlinear field generation by both plasma instabilities in the precursor (Lucek & Bell 2000; Bell 2004) and fluid-type instabilities in the downstream plasma (Giacalone & Jokipii 2007). These two mechanisms can, in principle, operate simultaneously (Zirakashvili & Ptuskin 2008). However, to reach the highest energies, particles must be speedily returned to the shock from excursions into both the upstream and downstream plasmas. The generation of an amplified magnetic field in the precursor that is subsequently advected into the downstream region is sufficient to ensure this, whereas amplification of only the downstream field is not.

Using a hybrid kinetic-MHD analysis, it was demonstrated by Bell (2004) that efficient cosmic-ray acceleration can, in the linear regime, drive a short wavelength, almost aperiodic, instability with wave-vector parallel to the ambient field. The growth of this mode can be considerably more rapid than that of the resonantly driven modes previously considered (McKenzie & Völk 1982; Achterberg 1983). The instability is driven by the reaction of the thermal plasma, as it attempts to compensate the current produced by the streaming cosmic rays. Numerical investigations of this instability have been performed using both MHD (Bell 2004, 2005; Reville et al. 2008; Zirakashvili et al. 2008) and Particle-In-Cell (PIC) simulations (Niemiec et al 2008; Riquelme & Spitkovsky 2008). While the results of MHD simulations show that the perturbed magnetic field δB becomes much larger than the initial uniform magnetic field B_0, the PIC simulations of Niemiec et al (2008) did not observe the parallel mode predicted in the linear analysis, and only moderate amplification of the magnetic field was observed. On the other hand, the recent results reported by Riquelme & Spitkovsky (2008) do identify the parallel mode and propose an explanation of its saturation in the non-linear stage.

In this paper we report new PIC simulations of this instability. We extend the range of parameters beyond that investigated by Niemiec et al (2008), and select values that more closely represent the environment in an SNR precursor. Although both 2D and 3D simulations in a similar parameter range have been performed (Riquelme & Spitkovsky 2008), we restrict our work to 2D. Our results — obtained independently and with some technical

differences in the numerical treatment — can be regarded as complementary, and our physical interpretation, at least of the early stages of the non-linear development, are congruent. In section 2, we recall the linear kinetic analysis of the nonresonant instability, in order to elucidate the conditions that must be satisfied in the PIC simulations. The details of our simulation parameters are described in section 3. We present the results of the simulations in section 4 followed by a discussion of the saturation and its implications in section 5. We conclude with a summary of the results.

2. Linear analysis

We review the linear kinetic analysis of an electron-ion plasma upstream of a non-relativistic shock with a power-law distribution of streaming cosmic rays. We focus our attention on parallel shocks, with the streaming velocity directed along the zeroth order magnetic field. The kinetic linear dispersion relation for circularly polarized hydromagnetic waves propagating parallel to the mean magnetic field in such a plasma was investigated by Achterberg (1983), subject to the conditions of zero net charge and current. In the upstream plasma frame the cosmic ray streaming velocity is approximately that of the shock velocity (McClements et al. 1996). Using the diffusion approximation it can be shown that, for a power-law momentum distribution of streaming cosmic rays with a spectral index $s > 3$ ($f_{\rm cr}(p) \propto p^{-s}$), the dispersion relation can be written as (Reville et al. 2007):

$$\omega^2 + \epsilon \left(\frac{k^2 V_{\rm ti}^2}{\Omega_{\rm ci}} \right) \omega - v_{\rm A}^2 k^2 - \epsilon \zeta v_{\rm s}^2 \frac{k}{r_{\rm g}} \left(\sigma(k r_{\rm g}) - 1 \right) = 0, \tag{1}$$

where $\omega = \omega_r + {\rm i}\gamma$ is the frequency of the waves in the upstream ion rest frame, $k > 0$ the wavenumber, $v_{\rm A}$ the Alfvén velocity, $V_{\rm ti}$ and $\omega_{\rm ci}$ the ion thermal velocity and cyclotron frequency, $v_{\rm s}$ the speed of the shock and $r_g = p_{\rm min} c / e B_0$ the gyroradius of the lowest energy cosmic ray. The polarization of the waves is determined by $\epsilon = +1(-1)$ for right (left) handed modes ($\omega_r > 0$). This result agrees with that found by Bell (2004) using an MHD approach, and extends it by including an additional term representing thermal ion damping. The growth rate of the unstable modes is determined by the driving parameter

$$\zeta = \frac{n_{\rm cr} p_{\rm min}}{n_{\rm i} m_{\rm i} v_{\rm s}}, \tag{2}$$

where $n_{\rm cr,i}$ are the densities of cosmic rays and ions. Finally σ is a complex function describing the electric fields produced by the cosmic ray current. It can be shown that σ is a decreasing function of wavenumber for $k r_{\rm g} > 1$ (Reville et al. 2007). In particular, for wavelengths much less than the gyroradius of the cosmic rays, σ can be neglected with respect to unity,

and one finds that there exists a purely growing mode with growth rate

$$\gamma_{\rm NR} = \frac{\zeta}{2}\frac{v_{\rm s}}{v_{\rm A}}\frac{v_{\rm s}}{r_{\rm g}} \approx \frac{1}{2}\frac{v_{\rm s}}{v_{\rm A}}\frac{n_{\rm cr}}{n_{\rm i}}\Omega_{\rm ci}. \tag{3}$$

An important constraint in deriving Eq. (1), is the magnetization condition, $|\omega| \ll \Omega_{\rm ci}$. On length scales much shorter than their gyroradius, the cosmic rays are essentially unmagnetized, i.e., their trajectories are rectilinear. The fact that the background plasma is magnetized leads to an asymmetry in the system, resulting in an uncompensated perpendicular current. This is what drives the growth or decay of all elliptical modes with $\mathbf{k}\cdot\mathbf{B_0} \neq 0$ (Bell 2005; Melrose 2005). If the background ions are unmagnetized, there is no inertia to support the growing waves, and the ions quickly act to compensate the cosmic-ray current. Significant heating of the plasma causes the ions to behave as if they were unmagnetized, thereby reducing the growth-rate. The same effect arises in the relativistic analysis of this instability (Reville et al. 2006).

In order to maintain a steady galactic cosmic-ray energy density, supernova remnants must channel approximately 10 percent of the kinetic energy entering the shock front into cosmic rays. Assuming a shock velocity of $v_{\rm s} = 0.01c$ with a cosmic-ray distribution $f_{\rm cr}(E) \propto E^{-2}$ from 10^7 eV to 10^{15} eV, this implies a cosmic-ray number density of $n_{\rm cr} = 10^{-5}\,{\rm cm}^{-3}$. Taking fiducial interstellar medium values for the ion number density and magnetic field: $n_{\rm i} = 1\,{\rm cm}^{-3}$ and $B = 3\ \mu$G, the maximum growth rate of the nonresonant instability is $\gamma_{\rm NR} \sim 2.5\times10^{-3}\Omega_{\rm ci}$. In the upstream rest frame, the cosmic rays drift with respect to the thermal ions at the shock velocity $v_{\rm s}$. To compensate this current, there is relative velocity between upstream ions and electrons, $V_{\rm d} = v_{\rm s}n_{\rm cr}/n_{\rm e} = 10^{-7}c$. This value is much smaller than the ion and electron thermal velocity. Hence an MHD description of the plasma is appropriate for the parameters in the precursor of a supernova remnant. P.I.C. simulations of this essentially MHD instability are computationally very intensive. However, they are the only way of quantifying the relative importance of high frequency waves and other kinetic effects on the nonlinear evolution of the instability.

3. Simulation

We use a 2D fully relativistic electromagnetic PIC code with a fast algorithm that solves for the current density and conserves charge (Umeda et al. 2003). The simulations are carried out in the upstream rest frame. While the simulations of Niemiec et al (2008) used a full kinetic treatment of the cosmic rays, during the linear stage of growth there was no significant reduction in the streaming energy of the cosmic rays. In order to identify the growth and evolution of the instability, we maintain a constant, uniform external cosmic-ray

current throughout the simulations, as has been used in previous MHD simulations (Bell 2004; Reville et al. 2008).

Similar to previous simulations, we investigate the role played by streaming cosmic rays of uniform density in a homogeneous electron-ion plasma. This is intended to represent a small region in the precursor of a supernova remnant shock. However, when, during the course of the simulation, the magnetic field fluctuations associated with the nonresonant instability become strong, they begin to damp the relative drift velocities of the cosmic rays and the gas. In a shock precursor, a change in relative drift velocity is automatically associated with an increase in the gas and cosmic ray densities, as the shock is approached. The simulation box, however, has periodic boundary conditions and, therefore, simulates a spatially uniform plasma. These boundary conditions therefore fail to reproduce the behavior expected in the shock precursor, as soon as the relative drift velocity changes significantly. For this reason, the saturation of the instability observed in the simulation, which occurs when the drift speeds become equal, does not correspond to the saturation mechanism expected in the shock precursor. However, the initial linear phase of the instability and a substantial part of its nonlinear evolution are accurately modelled.

3.1. Setting

We define the zeroth order magnetic field to be along the negative x-direction, and the cosmic rays stream in the positive x-direction. Periodic boundary conditions are used in both the x and y directions. The electrons, ions and cosmic rays are initialized such that the overall charge and current densities vanish. Thus, $n_{\rm e} = n_{\rm i} + n_{\rm cr}$ and the electrons have a net drift velocity in the x-direction of $V_{\rm d,e} = V_{\rm d,cr} n_{\rm cr}/n_{\rm e}$. (Subscripts e, i and cr represent electrons, ions and cosmic rays, respectively.) At the beginning of the simulation, each population is uniformly distributed in the $x-y$ plane with a Maxwellian momentum distribution at equal temperatures $T = T_{\rm e} = T_{\rm i} = 1.3$ keV. The length of each cell $\Delta x = \Delta y$ and time step Δt of the simulation are twice the Debye length and $0.0714\omega_{\rm pe}^{-1}$, respectively. Initially, each cell contains 49 positively and 49 negatively charged macroparticles. In the presence of a uniform cosmic ray density, the charge of each species of macroparticle must be chosen such that the overall plasma is initially charge neutral. The charge to mass ratio of the negatively charged macroparticles corresponds to that of an electron.

The values for $\Omega_{\rm ce}/\omega_{\rm pe}$, $n_{\rm cr}/n_{\rm i}$, $V_{\rm d}/c$ and the number of cells for each simulation run are given in Table 1, where $\Omega_{\rm ce}$ and $\omega_{\rm pe}$ are the electron cyclotron frequency and electron plasma frequency, respectively. We also specify the mass ratio $m_{\rm i}/m_{\rm e}$ for each run. To make the problem more tractable, we are forced to use unrealistically high values for the cosmic-ray

number densities. This is done purely to reduce the computation time, and, as we show, the essential physical mechanisms are still well-captured.

The size of the simulation box in the x and y-directions for run A is taken to be $L_x = L_y = 6.66\lambda_{\rm NR}$, where $\lambda_{\rm NR} = 2\pi v_{\rm A}/\gamma_{\rm NR}^{\rm max}$ is the wavelength of the most unstable mode of the nonresonant instability. The simulation is followed until $40\tau_{\rm grow}$, where $\tau_{\rm grow} = \gamma_{\rm NR}^{-1}$. The parameters used in run B are chosen such that the magnetization condition $\gamma_{\rm NR} < \Omega_{\rm ci}$ is not satisfied. As discussed in section 2, it is not expected that the nonresonant current-driven instability will operate in such a situation. Similar parameters have been used by Niemiec et al (2008), and we perform this simulation in order to facilitate comparisons with that work. The size of the simulation box for run-B is $L_x = L_y = 9.65\lambda_{\rm NR}$.

We also perform two additional simulations, runs C and D, with higher cosmic-ray drift velocity and mass ratio, respectively. The box size is the same as that used in run A, $L_x = L_y = 6.66\lambda_{\rm NR}$. While the conditions in run C are less appropriate for a supernova shock precursor than those of run A, the increased cosmic-ray drift speed provides a greater amount of free energy in the system. Likewise, the magnetization condition in run A is satisfied better than in run D, however, the larger mass ratio allows us to investigate the effect that increased inertia has on the thermal ions.

4. Results

The evolution of the spatially averaged energy density of the magnetic and electric field components associated with the growing waves, for run-A is shown in Figure 1. The linear growth rate of the spatially averaged transverse component of the magnetic field is approximately $\sim 0.5\gamma_{\rm NR}$. The characteristic wave length is almost the same as that predicted by the linear analysis. Figure 2a shows the spatial distribution of the $z-$component of magnetic field during the linear phase of growth ($t = 14\tau_{\rm grow}$)[1] , where the k-vector is clearly directed along the zeroth order field. The y-component of the magnetic field has a similar structure with the phase of the wave pattern shifted by $\pi/2$.

For comparison, we show in Figure 2b, the $z-$component of the magnetic field during the linear phase of growth for run-B. The ions in this case are not magnetized, and the nonresonant mode is not observed. The wave is aperiodic and its wavevector is almost perpendicular to the beam. This is typical of Weibel-type instabilities. We discuss this further in the next section.

[1]Note $t > \tau_{\rm grow}$ does not mean nonlinear phase because the initial perturbation is very small.

The linear development of the fluid quantities in the simulations is similar to that of previous MHD simulations Bell (2004, 2005); Reville et al. (2008); Zirakashvili et al. (2008). The initial stage sees the development of the aperiodic instability, with uniform density. As the fastest growing mode emerges from the initial noise, the net $\mathbf{j} \times \mathbf{B}$ force begins to push the plasma in the direction transverse that of the cosmic ray drift, generating low density regions between filaments of compressed plasma. The filaments are uncorrelated in the direction of the cosmic ray drift, similar to what is observed in MHD simulations (e.g. Bell 2004; Reville et al. 2008). The growth of the cavities is eventually limited due to the expansion of neighbouring cavities, at which point they appear to have a radius of $\lambda_{\rm NR}$.

The late-time nonlinear evolution, however, differs from that of previous MHD simulations. While both see the eventual disruption of the filamentary structures, the particle in cell simulations see an acceleration of the background plasma in the direction of the cosmic-ray drift. This effect is not observed in simulations that represent the system as a single MHD fluid driven by a fixed external current, because the charge of the streaming particles, and hence, the direction in which they drift, is undefined. Figures 3(a) and 3(b) show the distribution of the total magnetic field energy and upstream proton density at the end of the simulation ($t = 40\tau_{\rm grow}$). Locally, the amplification factor $\delta B/B_0$ is about 16 but the global, spatially averaged value is about 4. These images differ quite considerably from the nonlinear results presented in previous MHD simulations (Bell 2004; Zirakashvili et al. 2008), not only because of the net drift, but also due to the anti-correlation between the magnetic field and the plasma density (Figure 3(b)).

At the point at which the magnetic field ceases to grow, the bulk plasma is drifting with a constant velocity $v_{d,i} = 0.9 v_{d,cr} = 0.09c$. This is almost the shock velocity. The development of run C and run D are similar to that of run A. However, the saturated field values are slightly larger, since the initial amount of free energy available is larger in both cases. The growth of the different field components is plotted for run C and run D in Figures 4 and 5, respectively. We discuss the physical nature of the field saturation in the next section.

5. Discussion

We find that the nonresonant cosmic-ray driven instability develops in all cases where the background plasma is magnetized. From Figure 2(a) and 2(b), it can be seen that there are considerable differences between the results of run A and run B although the observed wavelength is similar to $\lambda_{\rm NR}$. The most unstable mode in run B is the Weibel type instability, occurring between the counterstreaming electrons and ions. Neglecting thermal effects and the magnetic field, the growth rate $\gamma_{\rm WI}^{\rm max}$ and the wavelength $\lambda_{\rm WI}$ of the Weibel instability

are

$$\gamma_{\rm WI}^{\rm max} = \frac{n_{\rm cr}}{n_{\rm e}}\frac{v_{\rm s}}{c}\omega_{\rm pi}, \quad \lambda_{\rm WI} = 2\pi\frac{c}{\omega_{\rm pe}}, \tag{4}$$

where the direction of the wave vector is perpendicular to the drift direction. Comparing the two theoretical growth rates and the wavelengths we see that

$$\frac{\gamma_{\rm WI}^{\rm max}}{\gamma_{\rm NR}^{\rm max}} = \frac{n_{\rm e}}{n_{\rm i}} \simeq 1, \quad \frac{\lambda_{\rm WI}}{\lambda_{NR}} = \frac{1}{2}\frac{n_{\rm cr}}{n_{\rm i}}\frac{V_{\rm d,cr}}{c}\frac{\omega_{\rm pe}}{\Omega_{ce}} \simeq 1. \tag{5}$$

For the choice of parameters used in run B, the wavelengths of the different instabilities are quite similar, even though the mechanism is quite different. This is consistent with the results of Niemiec et al (2008), and we also find the fastest growing mode to be slightly oblique. Hence we may be observing a mixed-mode between the Weibel and the nonresonant current driven instability or some other type of mixed-mode instability similar to those discussed in Bret et al. (2005).

In the late stages of the simulations we see the emergence of a non-thermal power law tail in the ion distribution. The use of a constant external cosmic-ray current prevents the development of the Buneman instability, a source of ion heating in the linear development. This dramatically reduces the heating in the initial stages, that was previously observed in Niemiec et al (2008). Figure 6 shows the final electron and ion energy distribution for run A, C and D. The distributions are essentially isotropic, and since the bulk drift velocity is small in comparision with the thermal velocities, we can safely calculate the spectrum in the box frame. The electron energy distribution can be well fitted with a Maxwellian distribution with temperature 10 keV for run A and 40 keV for run C and D. A non-thermal tail appears in the distribution of the ions with a very soft power-law index of ~ 7.3 for Run-A, but a relatively hard ~ 2 for run C and D. The mechanism responsible for the formation of this power-law distribution is not clear, and although our simulations have a relatively large number of particles per cell, we cannot rule out a numerical artefact. As regions of oppositely polarized magnetic field collide each other, an anti-parallel configuration of the magnetic fieldlines appears. It is, therefore, possible that collisionless magnetic dissipation may also play an important role in plasma heating mechanism and the saturation of the field growth as well as the reduction in the drift velocity between the electrons and ions. This is an interesting process in its own right, and further investigation is warranted. However, in the current context, it is not clear what role these mechanisms play, since the late-stage nonlinear behavior has no counterpart in the supernova-shock scenario.

In agreement with Niemiec et al (2008) and Riquelme & Spitkovsky (2008), we observe in our simulations that the magnetic field growth ceases when the plasma bulk velocity becomes comparable to the cosmic-ray drift velocity. Although we have fixed the cosmic ray current in our simulations, the observed saturation is clearly due to the reduction in

the relative speeds of plasma and cosmic rays. Indeed, if the cosmic rays are isotropic in the plasma frame, no streaming instability can operate. The simulations are performed in a box with periodic boundary conditions in space. The plasma speed is initially zero, and the cosmic ray streaming speed is maintained constant in time and space. It represents the speed with which the shock front approaches the simulation box. Within this picture, the instability can saturate only when the entire plasma moves with the drift speed of the cosmic rays.

In the precursor of a shock front, conditions are different. There, the interaction between plasma and cosmic rays defines the diffusion length scale of the cosmic rays. This is the scale on which the cosmic ray current, or, equivalently, pressure, decays with distance ahead of the shock front. In the case of efficient acceleration, it is also the length scale on which the precursor plasma is compressed. Simulations can model this situation provided the box size is small compared to the diffusion length scale, and the time scales are short compared to the time on which the cosmic ray current and plasma density change because of the approaching shock front. However, this restriction means that the simulations no longer model a precursor when they are followed until the plasma speed approaches the shock speed (which equals the cosmic-ray drift speed).

This can be seen explicitly from the equation of conservation of mass in a stationary precursor, $\rho(x)u(x) = \text{constant}$, which dictates that any change in the flow velocity must be associated with a change in the density of the fluid. In the present context, the simulation box is in the upstream plasma frame, approaching the shock with velocity v_s. Defining the density and bulk velocity inside the box to be ρ_b and u_b respectively, we see that

$$\rho_\mathrm{b} = \frac{v_\mathrm{s}\rho_0}{v_\mathrm{s} - u_\mathrm{b}} \tag{6}$$

where ρ_0 is the initial density of the thermal plasma. Thus, as the flow speed inside the box increases, the density should also increase. Since the total density in the box is fixed throughout the simulation, the observed growth rate is only accurate provided the bulk velocity inside the box is small compared to the shock velocity, or, equivalently, the streaming speed of the cosmic rays, i.e., $u_\mathrm{b} \ll v_\mathrm{s}$. This corresponds to $\tau_\mathrm{grow} < 20$ for run A and $\tau_\mathrm{grow} < 23$ for runs C and D. The amplification of the energy density in the total field in run A is not yet substantial, but in runs B and C roughly 10 times the initial energy density is reached. The final saturation levels are much higher, but our simulations do not necessarily imply that these can be reached in a precursor scenario, and a PIC simulation of this case is currently out of reach.

6. Summary

We have performed 2D PIC simulation to investigate the nonlinear physics of the nonresonant current instability. We have demonstrated that the energy in the growing waves can substantially exceed that of the initial seed field. However, limitations inherent in the simulation method lead to an artificial saturation level. Although we cannot compute a realisitic saturated value of the magnetic field, substantial amplification is seen in some runs before they lose validity, and the possibility remains open that the field would continue to grow, transferring the energy to longer lengthscales, in accordance with theoretical predictions. Thus, as predicted, magnetic field amplification is triggered by the nonresonant streaming instability and is likely to play an important role in the acceleration of cosmic rays to the knee and beyond in supernova remnants.

Y.O. is grateful to S. Matsukiyo and T. Umeda for discussions on the nonresonant instability and PIC simulations. B.R. thanks A. Spitkovsky for many useful discussions. Y.O. is supported by a Grant-in-Aid for JSPS Research Fellowships for Young Scientists. BR gratefully acknowledges support from the Alexander von Humboldt foundation. Numerical computations were carried out on the Cray XT4 at Center for computational Astrophysics, CfCA, of the National Astronomical Observatory of Japan and on the Blue Gene/P at the Rechenzentrum Garching of the Max Planck Society.

REFERENCES

Achterberg, A. 1983, A&A, 119, 274

Bamba, A., Yamazaki R., Yoshida T., Terasawa T., and Koyama, K., 2005, ApJ, 621, 793

Bell, A. R. 2004, MNRAS, 353, 550

Bell, A. R. 2005, MNRAS, 358, 181

Berezhko, E. G.,Astroparticle Physics, 5, 367

Berezhko, E. G., Ksenofontov, L. T., & Völk, H. J., A&A, 412, L11

Bret, A., Firpo, M.-C. & Deutsch, C. 2005 Phys. Rev. E, 72, 6403

Giacalone, J., & Jokipii, J.R., 2007, ApJ, 663, L41

Hillas, A. M. 2005, Journal of Physics G Nuclear Physics, 31, 95

Lagage, P. O. & Cesarsky, C. J. 1983, A&A, 125, 249

Lucek, S. G. & Bell, A. R. 2000, MNRAS, 314, 65

McClements, K. G., Dendy, R. O., Drury, L. O., Duffy, P., 1996, MNRAS, 280, 219

J.F. McKenzie, H.J. Völk, 1982 A&A, 116, 191

Melrose D., 2005, AIPC, 781, 135

Niemiec, J., Pohl, M., Stroman, T. & Nishikawa, K., 2008, ApJ, 684, 1174

Reville, B., Kirk, J. G., & Duffy, P., 2006, Plasma Physics and Controlled Fusion, 48, 1741

Reville, B., Kirk, J. G., Duffy, P. & O'Sullivan, S., 2007, A&A, 475, 435

Reville, B., O'Sullivan, S., Duffy, P. & Kirk, J. G., 2008, MNRAS, 386, 509

Riquelme, M. A. & Spitkovsky, A., 2008, astro-ph/0810.4565

Shapiro, V. D., Quest, K. B. & Okolicsanyi, M., 1998, Geophys. Res. Lett.25, 845

Uchiyama, Y., Aharonian, F A., Tanaka, T., Takahashi, T., & Maeda, Y., 2007, Nature, 449, 576

Umeda,T., Omura, Y., Tominaga, T., &Matsumoto, H. 2003, Comp. Phys. Comm., 156, 73

Vink, J. & Laming, J. M. 2003, ApJ, 584, 758

Zirakashvili, V. N., & Ptuskin, V. S. 2008, ApJ, 678, 939

Zirakashvili, V. N., Ptuskin, V. S. & Völk, H. J. 2008, ApJ, 678, 255

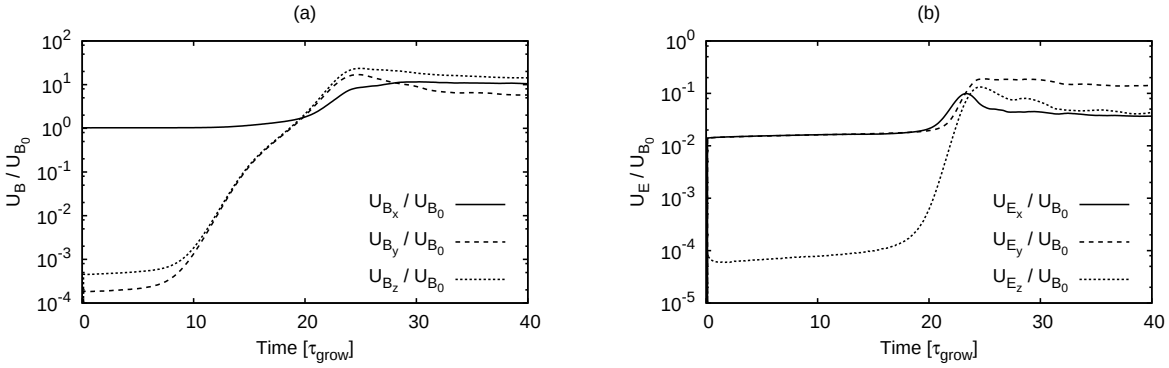

Fig. 1.— Time development of the spatially averaged root mean square of (a) magnetic field, (b) electric field for Run-A. Solid, dashed and dotted curves represent the x, y and z-components, respectively.

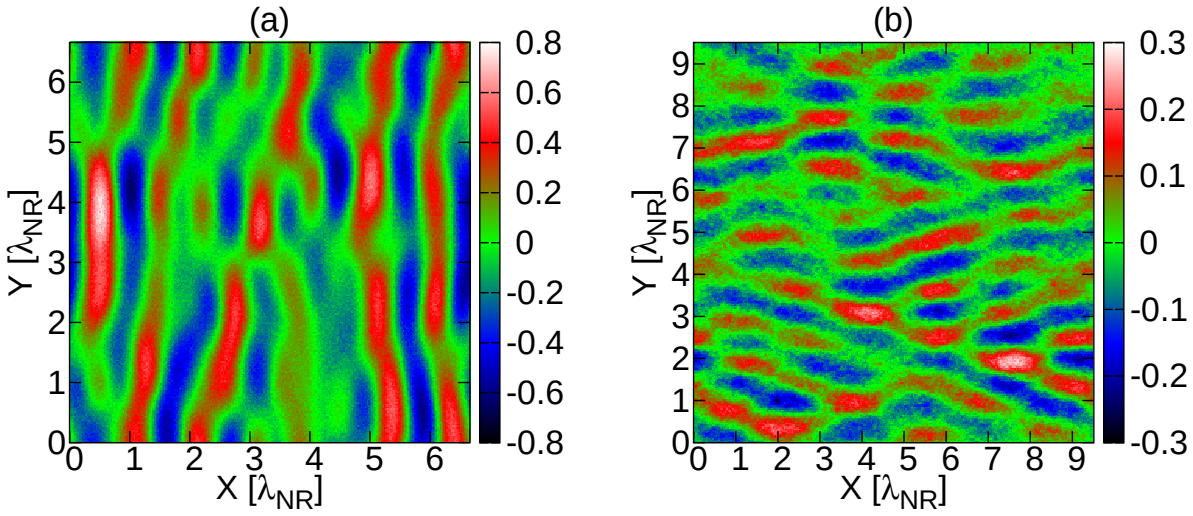

Fig. 2.— z-component of magnetic field at (a) $t = 14\tau_{\rm grow}$ in run-A, (b) $t = 8\tau_{\rm grow}$ in run-B.

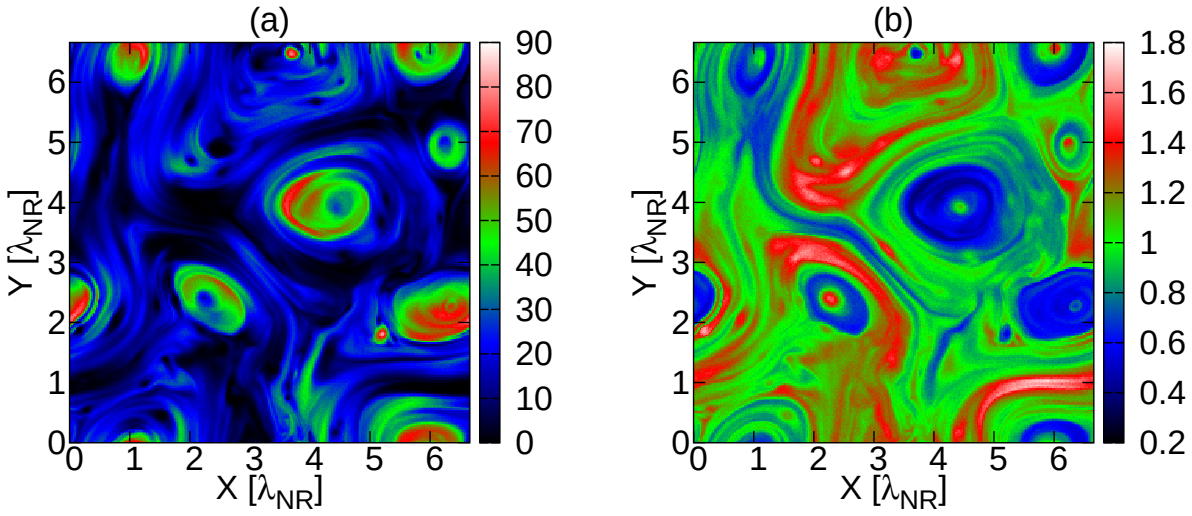

Fig. 3.— (a) The magnetic field energy density, and (b) density of ions at $t = 40\tau_{\rm grow}$ in run-A

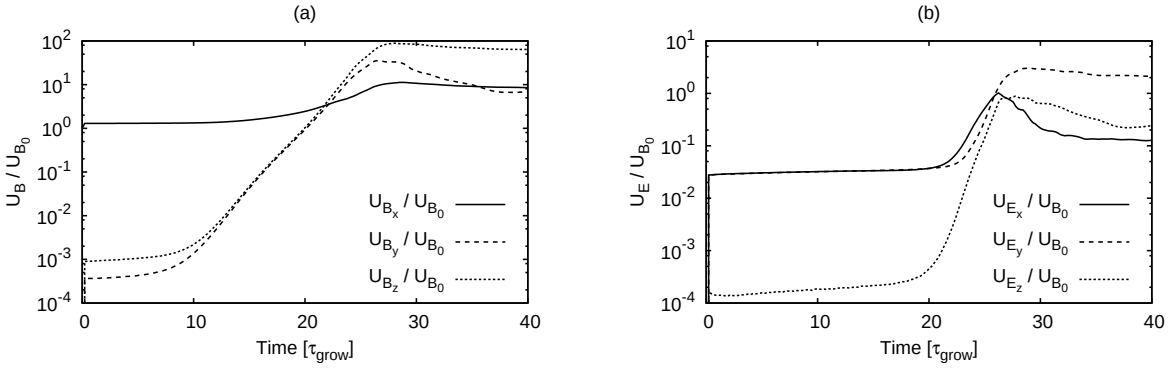

Fig. 4.— Time development of the spatially averaged root mean square of (a) magnetic field, and (b) electric field for Run-C. Solid, dashed and dotted curves represent the x, y and z-components, respectively.

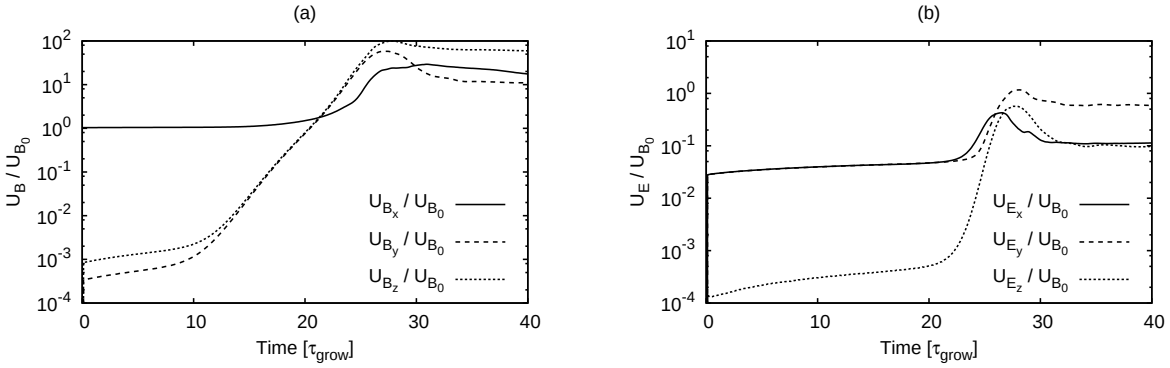

Fig. 5.— Time development of the spatially averaged root mean square of (a) magnetic field, and (b) electric field for Run-D. Solid, dashed and dotted curves represent the x, y and z-components, respectively.

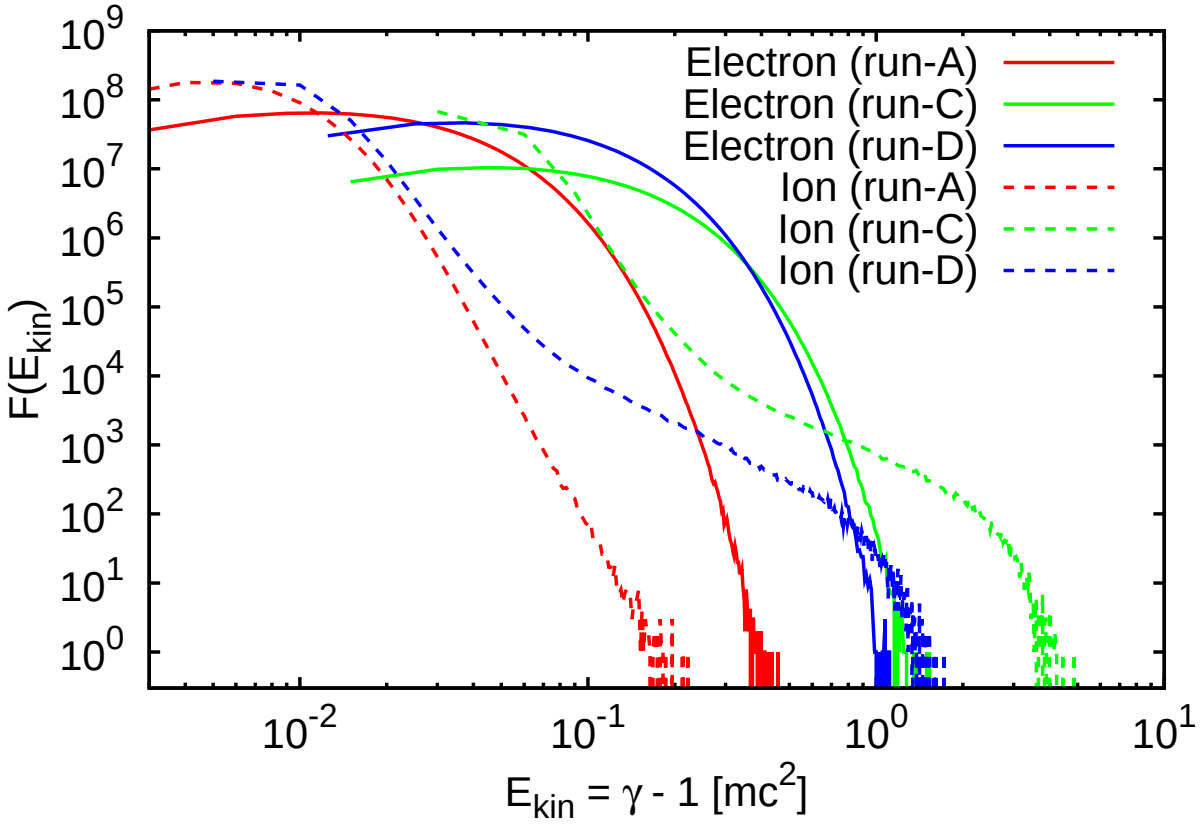

Fig. 6.— Energy distribution at the final stage in run-A, C and D

Table 1. Simulation Parameters

Run	$\Omega_{\rm ce}/\omega_{\rm pe}$	$m_{\rm i}/m_{\rm e}$	$n_{\rm cr}/n_{\rm i}$	$V_{\rm d,cr}/c$	cell
A	3.26×10^{-2}	10	1/20	0.1	4096×4096
B	4.52×10^{-2}	10	1/3	0.3	512×512
C	3.26×10^{-2}	10	1/20	0.2	2048×2048
D	3.26×10^{-2}	40	1/20	0.1	4096×4096

Note. — Parameters of the simulation runs described in this paper. Listed are: the ratio of electron cyclotron frequency and electron plasma frequency $\Omega_{\rm ce}/\omega_{\rm pe}$, ion-electron mass ratio $m_{\rm i}/m_{\rm e}$, the density ratio of ambient ions and cosmic rays $n_{\rm cr}/n_{\rm i}$, the velocity ratio of cosmic-ray drift and light speed $V_{\rm d,cr}/c$, the cell number